nature physics

ARTICLES

https://doi.org/10.1038/s41567-019-0480-1

The microscopic role of deformation in the dynamics of soft colloids

Nicoletta Gnan* and Emanuela Zaccarelli*

Soft colloids enable the exploration of states with densities exceeding that of random close packing, but it remains unclear whether softness controls the dynamics under these dense conditions. Experimental studies have reported conflicting results, and numerical studies have so far focused primarily on simple models that allow particles to overlap, but neglect particle deformations. This makes the concept of softness in simulations and experiments difficult to compare. Here, we propose a model system consisting of polymer rings with internal elasticity. At high packing fractions, the system displays compressed exponential decay of the intermediate scattering functions and super-diffusive behaviour of the mean-squared displacements. These features are explained in terms of the complex interplay between particle deformations and dynamic heterogeneities, which gives rise to persistent motion of ballistic particles. We also observe a striking variation of the relaxation times with increasing particle softness, clearly demonstrating the crucial role of deformation in the dynamics of realistic soft colloids.

In recent years, colloidal particles have emerged as useful models that give access to phases and states with no counterpart in atomic and molecular systems[1–3]. In addition they have allowed the establishment of new mechanisms to control phase behaviour[4–6] and to deepen our understanding of the glass and jamming transition[7–9]. A crucial parameter controlling colloidal behaviour is particle softness, which can be quantified by the ratio between elastic and thermal energy[10]. Hence, particle internal elasticity is the key ingredient to distinguish hard particles like sterically stabilized polymethylmethacrylate colloids from soft and ultrasoft ones such as microgels, emulsions or star polymers, to name a few. Several experimental works[9,11–13] have reported that softness controls the dependence of the structural relaxation time τ_α on temperature T or on packing fraction ζ—the so-called fragility[14]. A system is called fragile when the τ_α dependence is described by a Vogel–Fulcher–Tammann law[15], meaning that its variation is large over small changes of T or ζ; in contrast, strong systems are characterized by an Arrhenius behaviour, implying a mild variation of τ_α on varying the control parameter. Although the pioneering study of Mattsson and colleagues[9] proposed a link between elasticity and fragility, there is still no consensus on this issue. A recent work based on a simple theoretical model has confirmed that such a link exists[16], but this picture was later challenged by experiments on colloids of different softness[17]. To gain microscopic knowledge on this matter we usually resort to simulations of simple repulsive models, such as systems interacting with the Hertzian potential[18], which is found to describe the behaviour of microgel particles at moderate packing fractions[19,20], but is expected to fail in denser conditions where soft colloids tend to shrink, deform or even interpenetrate[21]. Early works have indicated that, for such simple pair potentials, the change of dynamic properties with softness, such as the change in fragility, is modest[22] or absent[23]. In these approaches, softness is tuned by modifying a given parameter, for example the strength of the repulsion, allowing particles to overlap to a certain extent, but without taking into account their deformability as well as other important aspects in realistic soft particles, namely deswelling[24–27], interpenetration[21] and faceting[28]. There is thus a strong need to go one step forward in the modelling of soft colloids to tackle this problem and to provide a microscopic picture of these systems at high densities.

To try to reconcile experimental and numerical results, in this work we investigate a new model of elastic polymer rings (EPRs) that explicitly shrink and deform. Inspired by recent experiments on ultrasoft microgels with tunable internal elasticity[29,30], we add a Hertzian potential of repulsive strength U (equation (3)) in the centre of mass of the polymer rings (Fig. 1a). This term allows the rings to retain a circular shape at low ζ but also provides an energetic cost associated with particle deformation. We perform two-dimensional (2D) extensive numerical simulations of polydisperse rings on varying U for a wide range of ζ up to very dense states, where faceting effects become important (Supplementary Fig. 1 and Supplementary Video 1). More details on the model are provided in the Methods.

We report in Fig. 1b the self-intermediate scattering functions $F_s(q^\star,t)$ for wavenumber $q^\star$, which corresponds to the maximum of the static structure factor, for different packing fractions ζ and a fixed value of the amplitude of the Hertzian potential $U=1{,}000$. The associated relaxation time τ_α, shown in Fig. 1c, at first increases, indicating a slowing down of the dynamics up to $\zeta=\zeta_R\approx0.9$. Above this packing fraction the system becomes faster as a result of melting upon compression, for all studied U values. Such a reentrant behaviour has already been observed for Hertzian spheres[31] and in simulations of single-chain nanoparticles[32], and it is confirmed here for 2D Hertzian disks (HZDs), as reported in the Supplementary Information. Although reentrant melting occurs both in EPRs and HZDs, its mechanism is very different in the two cases: HZDs do this by overlapping, while EPRs through particle deformation, which is accompanied by the accumulation of internal stresses. This difference is encoded in the shape of $F_s(q^\star,t)$, which is described by the shape parameter β defined in equation (4): the decay of $F_s(q^\star,t)$ always has a stretched exponential form ($\beta<1$) for HZDs, as also shown in Supplementary Fig. 2, while for EPRs it becomes faster than exponential ($\beta>1$) for $\zeta\gtrsim\zeta_R$, as shown in Fig. 1d. This signals the onset of a compressed exponential relaxation

CNR-ISC (National Research Council – Institute for Complex Systems) and Department of Physics, Sapienza University of Rome, Rome, Italy.
*e-mail: nicoletta.gnan@roma1.infn.it; emanuela.zaccarelli@cnr.it

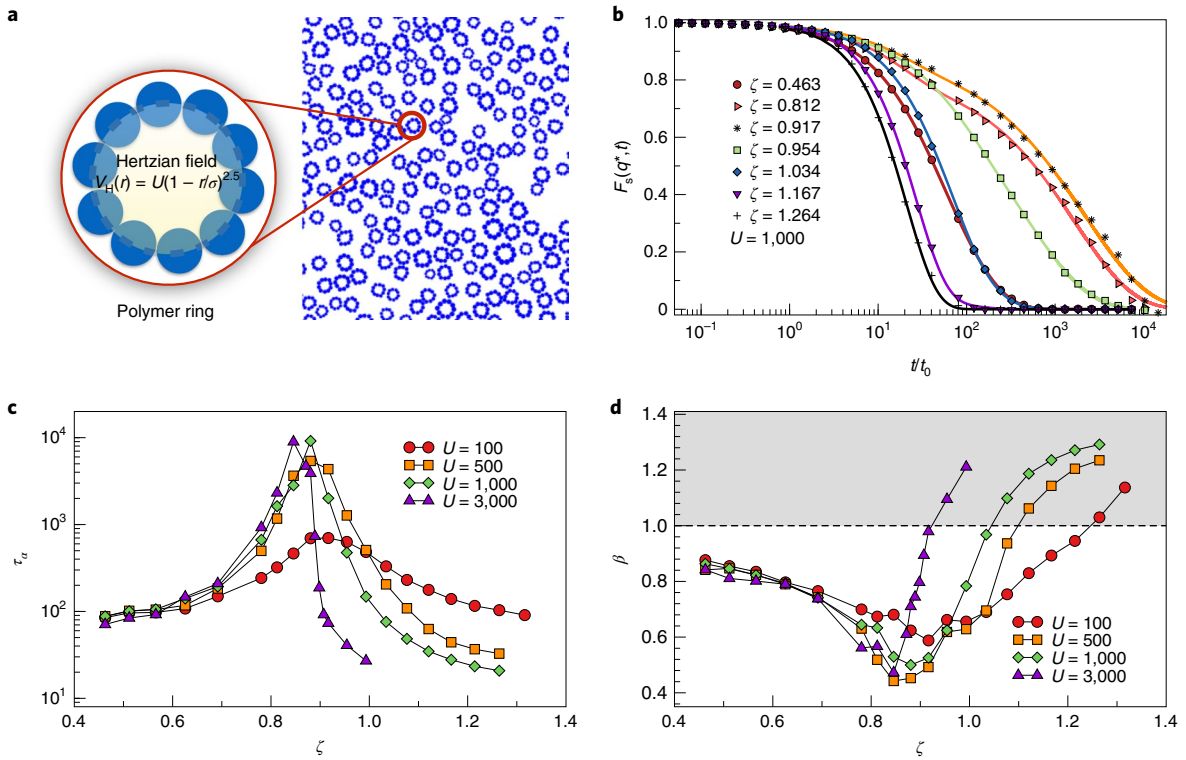

Fig. 1 | Model system and dynamic properties as a function of packing fraction. a, Snapshot of a portion of EPRs with $U=1{,}000$ and $\zeta=0.463$ and illustration of the model. Representative snapshots at different ζ values are reported in Supplementary Fig. 1. **b**, Self-intermediate scattering function $F_s(q^*,t)$ for EPRs with $U=1{,}000$. Symbols are simulation data and solid lines are fits using equation (4). **c**,**d**, Relaxation time τ_α (**c**) and shape parameter β (**d**) extracted from the fits to $F_s(q^*,t)$ for rings with different U. In **d**, the grey area highlights the compressed exponential region.

of the density autocorrelation functions, found for all studied U (Supplementary Fig. 3), with β values strongly dependent on softness and on ζ.

The compressed exponential decay of $F_s(q^*,t)$ for $\zeta \gtrsim \zeta_R$ is accompanied by a super-diffusive behaviour of the mean-squared displacement (MSD), that is $\langle r^2(t)\rangle \sim t^\gamma$ with $\gamma>1$, as shown in Fig. 2a. This holds in an intermediate time window of about two decades, while, at long times, the MSD always becomes diffusive again. Similar results are found for all studied values of U with the exponent γ depending on ζ and U (Supplementary Fig. 4), in analogy with the shape parameter β.

To grasp the microscopic origin of the observed compressed/super-diffusive behaviour and the associated exponents, we analyse the system in terms of dynamic heterogeneities. We thus monitor the dynamics of fast particles at high ζ in a time window Δt of the order of τ_α (see Methods). We find that the MSD of fast particles, averaged over several time windows, displays a super-diffusive behaviour such as the total one, albeit with a significantly higher exponent. We separately analyse different time windows and find that, for a large number of them (see Methods), the MSD of the fastest particles obeys a purely ballistic dynamics, that is $\langle r^2(t)\rangle \sim t^2$ in the considered time interval (Fig. 2b). At long times, they still recover diffusive behaviour.

Further insights can be gained by looking at $F_s(q^*,t)$ for the same selected fastest particles, as shown in Fig. 2c, which displays a compressed exponential decay with exponent $\beta=2$ in the same time window. We also carried out a similar analysis for different values of ζ and U and found that these features are preserved but the number of fastest particles showing ballistic behaviour varies; in particular, it increases with ζ and U. This allows us to explain the observed anomalous dynamics in terms of a superposition of different particle populations, including groups of ballistic particles whose size depends on softness and packing fraction, reflecting the increase of exponents β and γ with U and ζ.

Interestingly, at long times, $F_s(q^*,t)$ becomes negative (Fig. 2c) before eventually decaying to zero. This intriguing behaviour has also been observed in active particles[33,34] and is the signature of a persistent motion of particles in a preferential direction. Indeed, it can be shown[35] for non-interacting ballistic particles moving with velocity v in the same direction that $F_s(q,t) \sim J_0(qvt)$, that is, a Bessel function of zeroth order.

The compressed exponential relaxation is still an important open question in colloidal systems and glass-formers[36–39]. Previous works on colloidal gels have linked the presence of such a feature to the accumulation of local stresses, which are then released into the system, triggering the faster-than-exponential dynamics[36,40–42]. Recent simulations have investigated this process by artificially altering the network dynamics[43] to observe stress propagation into the system. However, no evidence has been provided so far of compressed exponential relaxation in a microscopic model undergoing spontaneous relaxation (in equilibrium), such as the present one.

By taking into account particle deformation in our model we are now able to quantify the local stress and to connect it to the onset of the compressed exponential behaviour. To this aim we define the asphericity parameter a (see Methods) that describes the deviation of the ring shape from a circular one (larger values of a correspond to more deformed particles). The distributions of particle asphericity $P(a)$ (Supplementary Fig. 5) indicate that, with increasing ζ, a larger and larger fraction of particles undergo strong deformation. A direct link exists between particle deformation and intra-ring stress, as discussed in the Supplementary Information (Supplementary Fig. 6). To quantify the effect of deformations at high ζ, we

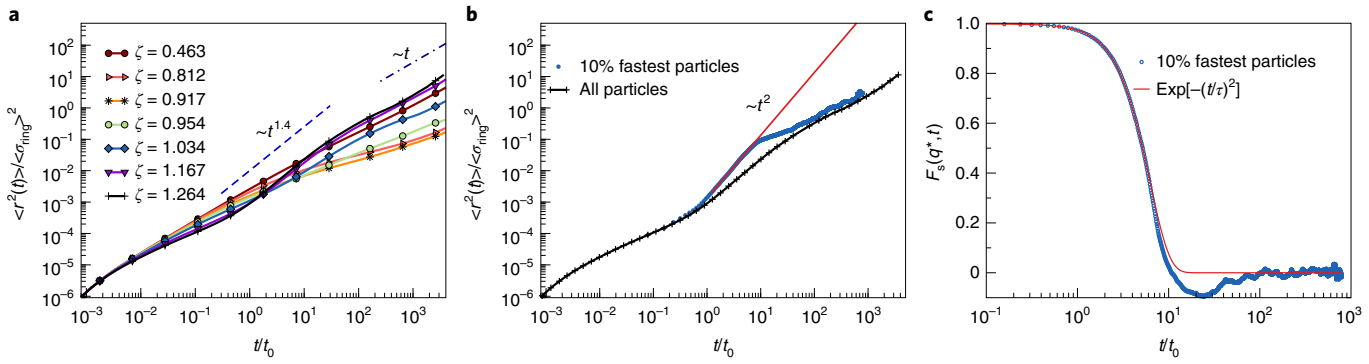

Fig. 2 | Mean-squared displacements and ballistic particles. a, MSD $\langle r^2(t)\rangle$ for EPRs with $U=1{,}000$ at different ζ. Lines are guides to the eye to show super-diffusive behaviour $\langle r^2(t)\rangle \sim t^{\gamma}$ (dashed) and normal diffusion at long times (dot-dashed). **b**, MSD of all particles (solid black line with symbols) and of ballistic fastest particles (blue symbols), detected in a time interval $\Delta t=7.88$ in reduced units, for $U=1{,}000$ and $\zeta=1.264$. The solid line is a power-law fit to the data yielding $\gamma=2.003\pm0.004$. **c**, $F_s(q^*,t)$ for ballistic fastest particles (symbols). The solid line is a compressed exponential fit to the data, yielding $\beta=2.019\pm0.012$.

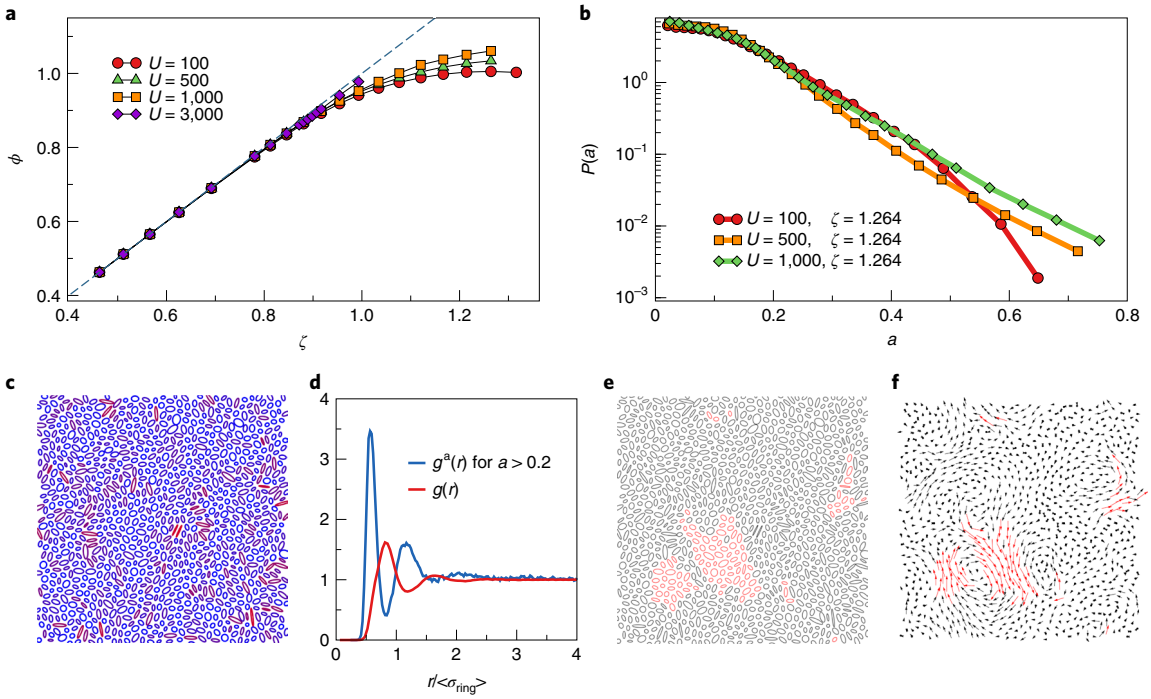

Fig. 3 | Analysis of deformation of rings. a, Effective packing fraction ϕ versus nominal packing fraction ζ for all investigated U values. **b**, $P(a)$ for $\zeta=1.264$ and different U values. **c**, Snapshot of EPRs represented as ellipses whose semi-axes correspond to the eigenvectors of the gyration tensor. **d**, Radial distribution functions $g(r)$ (for all rings) and $g^a(r)$ (for strongly deformed rings with $a>0.2$) for $U=1{,}000$ and $\zeta=1.264$. **e**,**f**, Same snapshot as in **d** highlighting in red the ballistic fastest particles in time interval $\Delta t=7.88$ in reduced units (**e**) and the associated displacements in the same time interval (**f**). The displacements are magnified (by an arbitrary factor) to improve visualization.

calculate the effective packing fraction ϕ occupied by the rings (see Methods), as shown in Fig. 3a. We find that ϕ coincides with the nominal packing fraction ζ for $\zeta \lesssim \zeta_R$, while it becomes significantly smaller than ζ for denser states. Softer particles show earlier deviations from the linear $\phi-\zeta$ relation than stiffer particles, as observed in experiments for ionic microgels[44]. Finally, for very large ζ, a strong bending of ϕ is detected, resulting even in a non-monotonic behaviour for the softest rings. These findings clearly indicate that our simple model is able to capture another of the main ingredients of realistic soft particles, that is, deswelling at high concentrations (due to shape deformation).

We now examine the variation of $P(a)$ with softness in Fig. 3b; while one may have expected to find stronger deformations in softer rings, this turns out not to be the case. Indeed, stiffer rings are found to display a longer tail for large a values. This is counteracted by the fact that, for a wide range of intermediate a values, $P(a)$ is larger for softer rings (for example, $U=100$). Thus, soft EPRs prefer to undergo a large spread of moderate deformations avoiding too high a values, while stiffer ones tend to accumulate strong deformations within a small fraction of rings (for example, $U=500$). When U increases even further, intermediate deformations also grow (for example, $U=1{,}000$). To understand the correlation between

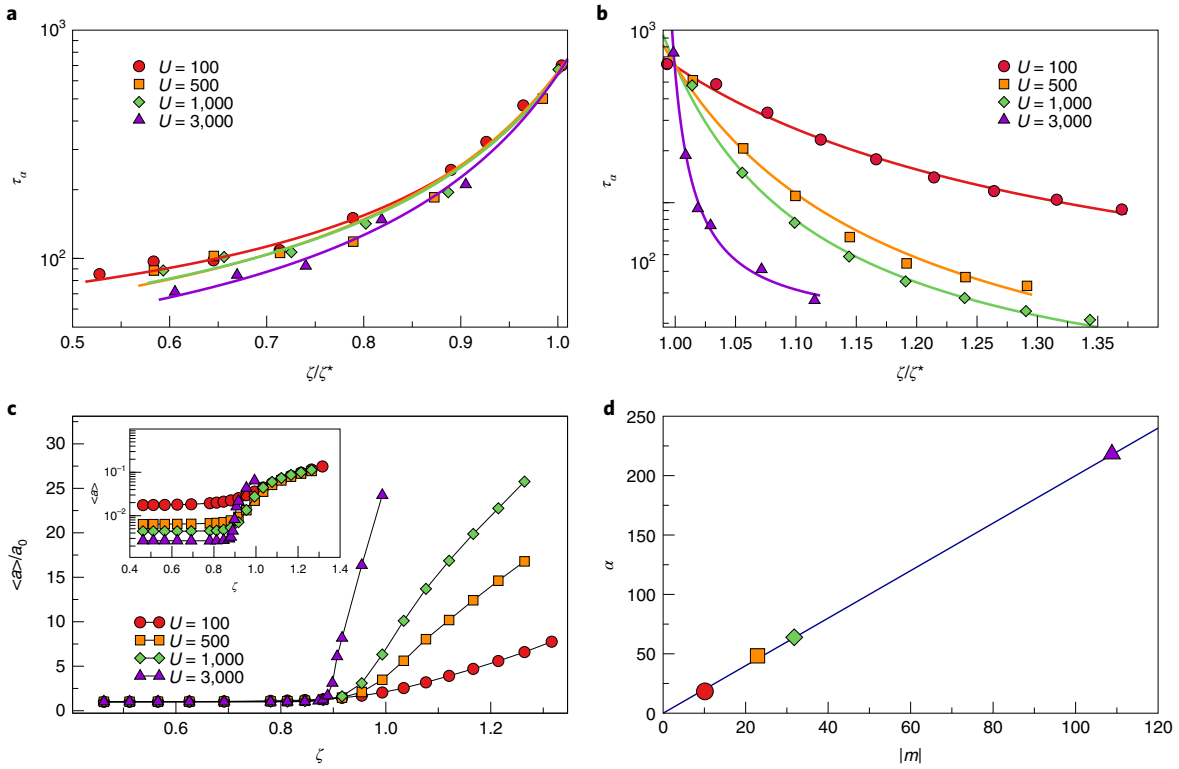

Fig. 4 | Softness-dependent fragility. a,**b**, Modified Angell's plots of the relaxation time τ_α below (**a**) and above (**b**) melting. For each U we define ζ^* as the packing fraction where $\tau_\alpha \simeq 650$ in reduced units. **c**, Average asphericity $\langle a \rangle$, normalized by its low density value $a_0 = \langle a(\zeta = 0.463) \rangle$, as a function of ζ for all investigated U. Inset: the same data without the low-density normalization. **d**, Absolute value of the fragility m as a function of the asphericity variation α.

deformation and dynamics, we calculate the autocorrelation function of the asphericity, and thus indirectly of the stress, as shown in Supplementary Fig. 7, and find that its relaxation time τ_{asph} roughly coincides with that at which the super-diffusive behaviour terminates. This result clearly connects the stress-releasing and stress-building mechanism with the occurrence of ballistic motion; within τ_{asph}, deformed particles release stress (reducing their asphericity) and contribute, with all other particles, to triggering the motion of less stressed particles. Because this is a mechanism involving the whole system, it is difficult to completely isolate each contribution, but our findings strongly suggest that stress-governing events entirely control the onset of the ballistic motion and the associated compressed exponential relaxation. Thus, in analogy with colloidal gels, the underlying physical mechanism of the compressed/super-diffusive dynamics is stress propagation, spontaneously obtained within our model through particle deformation.

To visualize how deformation and stress are distributed within the system, a snapshot of EPRs with $U = 1{,}000$ at the highest investigated ζ is reported in Fig. 3c, where each ring is represented by an ellipse based on the eigenvectors of its gyration tensor. It is evident that deformed particles tend to stay close to each other, generating strings of elongated ellipses that surround areas of less deformed/less stressed particles. This is quantified by the radial distribution function $g^a(r)$ of rings with large asphericity (that is, $a > 0.2$), which displays a higher peak located at smaller distances with respect to the average $g(r)$, as shown in the inset of Fig. 3d. The same snapshot is also shown in Fig. 3e, which highlights the fastest ballistic rings; remarkably, these are found in very large clusters. Furthermore, not only are their positions correlated, but also their displacements (Fig. 3f). A high degree of alignment in the direction of motion is clearly present, in full agreement with the observation of a negative oscillation in $F_s(q^*, t)$ (Fig. 2c). On the boundary of these clusters, slower rings that are either more deformed or are moving in a different direction physically stop the ballistic motion of the fastest particles, which are then slowed down until recovering normal diffusion (Fig. 2b). This happens when particle deformations in the system are able to finally relax (Supplementary Fig. 7). The fact that the stress continuously propagates through the system is qualitatively illustrated in the stress maps reported in Supplementary Fig. 8 for different times and can be better visualized in Supplementary Video 1. This phenomenology is completely missing in HZDs (Supplementary Fig. 9), where stress is absent and particle overlaps are spread out, so no persistent motion is observed.

The results derived so far show that particle deformations give rise to large dynamical heterogeneities that result in an intermittent collective motion of portions of particles that move ballistically. We then address how deformation, and hence particle softness, influences the behaviour of τ_α as a function of ζ. With this aim we report a modified Angell's plot[14] of the relaxation time in Fig. 4, obtained as discussed in the Methods, both above and below ζ_R. Interestingly, we find that for $\zeta < \zeta_R$, τ_α is almost independent of softness (Fig. 4a), while for $\zeta > \zeta_R$ a striking variation of the relaxation time with ζ is found (Fig. 4b). In this regime, a transition from fragile behaviour at large stiffness to (quasi)-strong behaviour for soft rings is observed, the latter being characterized by an almost Arrhenius dependence of τ_α on ζ/ζ^*. Because this transition only occurs above melting, when particles are strongly compressed, a clear connection must exist between softness (in terms of the single-particle elastic properties) and fragility, the latter here defined as $m = [\mathrm{d}\ (\ln \tau_\alpha)/\mathrm{d}(\zeta/\zeta^*)]\ |_{\zeta=\zeta^*}$ in analogy with that of standard glassy systems. In our model, softness is intimately related to particle deformation. We thus test whether a connection between

deformation and fragility also exists. The average asphericity $\langle a \rangle$, normalized by its low-ζ value a_0, is shown as a function of ζ in Fig. 4c. Clearly, for $\zeta < \zeta_R$, $\langle a \rangle$ changes very little, although it varies significantly for different U (inset of Fig. 4c). However, for $\zeta \gtrsim \zeta_R$, the variation of $\langle a \rangle$ becomes much larger for stiffer rings. The fragility is plotted against the variation of the average asphericity $\alpha = (\mathrm{d}\langle a \rangle / \mathrm{d}\zeta)|_{\zeta=\zeta^*}/a_0$ in Fig. 4d for $\zeta \gtrsim \zeta_R$. A linear relation between the two quantities is found for all investigated values of U, confirming that in our model a change of the single-particle internal elasticity affects the fragility of the system.

The microscopic origin of fragility in soft colloids has remained mostly elusive so far. Several experiments have reported evidence of a fragility variation[9,11–13], and a simple theoretical model[16] recently showed that the osmotic regulation of compressible particles can describe a fragile-to-strong transition when the nominal packing fraction ζ is used. In ref. [16] this was shown to derive from the strong nonlinear relationship between ζ and ϕ, which always gives rise to a fragile behaviour when the Angell's plot is represented as a function of ϕ. Hence, the observed fragility variation was interpreted as being only an apparent one. However, such a model[16] as well as subsequent simulations[27] did not take into account particle deformation. Instead, in the present study the microscopic connection between deformation and fragility, highlighted in Fig. 4d, induces a variation in fragility at high densities, also when the modified Angell's plot is shown as a function of ϕ, as reported in Supplementary Fig. 10.

It is worth noting that refs. [9,12,13] deal with interpenetrated network microgels where charge effects such as ion-induced deswelling may be relevant, a situation far more complex than what can be described by our simple model. However, our work sheds light on recent experiments[17] for standard microgels and charged colloids, which reported no fragility variation on increasing ζ in the same region where we also do not detect it, that is, for $\zeta < \zeta_R$. We find that it is only for $\zeta > \zeta_R$, in a regime where the rings are clearly compressed and deformed, that this variation should be detected. It may therefore be necessary to probe highly dense conditions, where particles are in direct contact with each other, to observe this behaviour. For this regime an increase in the shape parameter β was also reported in ref. [17], in agreement with the present findings, but the occurrence of solid-like behaviour preempts the investigation of the system at even higher densities. In this respect, softness is truly a valuable parameter, because, in principle, highly dense states could be accessed in equilibrium for much softer systems. With this in mind, ultrasoft microgels—that is, microgels without or with very few crosslinkers[29,30,45]—as well as hollow microgels[46], for which an empty core is surrounded by a fluffy polymeric corona, may be suitable candidates with which to verify the present results. Our EPR model was indeed inspired by these systems, offering a simple 2D schematization of the particles, but still retaining the minimal ingredients to describe complex phenomena at high densities, such as particle deswelling and faceting. Its 3D investigation will thus be a natural extension of this work.

Online content

Any methods, additional references, Nature Research reporting summaries, source data, statements of data availability and associated accession codes are available at https://doi.org/10.1038/s41567-019-0480-1.

Received: 17 June 2018; Accepted: 20 February 2019;
Published online: 01 April 2019

References

1. Ruzicka, B. et al. Observation of empty liquids and equilibrium gels in a colloidal clay. *Nat. Mater.* **10**, 56–60 (2011).
2. Dotera, T., Oshiro, T. & Ziherl, P. Mosaic two-lengthscale quasicrystals. *Nature* **506**, 208–211 (2014).
3. Chen, Q., Bae, S. C. & Granick, S. Directed self-assembly of a colloidal kagome lattice. *Nature* **469**, 381–384 (2011).
4. Hertlein, C., Helden, L., Gambassi, A., Dietrich, S. & Bechinger, C. Direct measurement of critical Casimir forces. *Nature* **451**, 172–175 (2008).
5. Sacanna, S., Irvine, W. T., Rossi, L. & Pine, D. J. Lock and key colloids through polymerization-induced buckling of monodisperse silicon oil droplets. *Soft Matter* **7**, 1631–1634 (2011).
6. van Anders, G., Ahmed, N. K., Smith, R., Engel, M. & Glotzer, S. C. Entropically patchy particles: engineering valence through shape entropy. *ACS Nano* **8**, 931–940 (2013).
7. Pham, K. N. et al. Multiple glassy states in a simple model system. *Science* **296**, 104–106 (2002).
8. Royall, C. P., Williams, S. R., Ohtsuka, T. & Tanaka, H. Direct observation of a local structural mechanism for dynamic arrest. *Nat. Mater.* **7**, 556–561 (2008).
9. Mattsson, J. et al. Soft colloids make strong glasses. *Nature* **462**, 83–86 (2009).
10. Vlassopoulos, D. & Cloitre, M. Tunable rheology of dense soft deformable colloids. *Curr. Opin. Colloid Interface Sci.* **19**, 561–574 (2014).
11. Seekell, R. P. III, Sarangapani, P. S., Zhang, Z. & Zhu, Y. Relationship between particle elasticity, glass fragility, and structural relaxation in dense microgel suspensions. *Soft Matter* **11**, 5485–5491 (2015).
12. Nigro, V. et al. Dynamical behavior of microgels of interpenetrated polymer networks. *Soft Matter* **13**, 5185–5193 (2017).
13. Nigro, V. et al. Structural relaxation, softness and fragility of IPN microgels. Preprint at https://arxiv.org/abs/1807.01692 (2018).
14. Angell, C. A. Formation of glasses from liquids and biopolymers. *Science* **267**, 1924–1935 (1995).
15. Debenedetti, P. G. & Stillinger, F. H. Supercooled liquids and the glass transition. *Nature* **410**, 259–267 (2001).
16. van der Scheer, P., van de Laar, T., van der Gucht, J., Vlassopoulos, D. & Sprakel, J. Fragility and strength in nanoparticle glasses. *ACS Nano* **11**, 6755–6763 (2017).
17. Philippe, A.-M. et al. Glass transition of soft colloids. *Phys. Rev. E* **97**, 040601 (2018).
18. Landau, L. D. & Lifshitz, E. *Theory of Elasticity* 3rd edn, Vol. 7, 109 (Course of Theoretical Physics, Butterworth-Heinemann, 1986).
19. Mohanty, P. S., Paloli, D., Crassous, J. J., Zaccarelli, E. & Schurtenberger, P. Effective interactions between soft-repulsive colloids: experiments, theory, and simulations. *J. Chem. Phys.* **140**, 094901 (2014).
20. Bergman, M. J. et al. A new look at effective interactions between microgel particles. *Nat. Commun.* **9**, 5039 (2018).
21. Mohanty, P. S. et al. Interpenetration of polymeric microgels at ultrahigh densities. *Sci. Rep.* **7**, 1487 (2017).
22. Sengupta, S., Vasconcelos, F., Affouard, F. & Sastry, S. Dependence of the fragility of a glass former on the softness of interparticle interactions. *J. Chem. Phys* **135**, 194503 (2011).
23. De Michele, C., Sciortino, F. & Coniglio, A. Scaling in soft spheres: fragility invariance on the repulsive potential softness. *J. Phys. Condens. Matter* **16**, L489–L494 (2004).
24. Urich, M. & Denton, A. R. Swelling, structure, and phase stability of compressible microgels. *Soft Matter* **12**, 9086–9094 (2016).
25. De Aguiar, I. B. et al. Deswelling and deformation of microgels in concentrated packings. *Sci. Rep.* **7**, 10223 (2017).
26. Weyer, T. J. & Denton, A. R. Concentration-dependent swelling and structure of ionic microgels: simulation and theory of a coarse-grained model. *Soft Matter* **14**, 4530–4540 (2018).
27. Higler, R. & Sprakel, J. Apparent strength versus universality in glasses of soft compressible colloids. *Sci. Rep.* **8**, 16817 (2018).
28. Conley, G. M., Aebischer, P., Nöjd, S., Schurtenberger, P. & Scheffold, F. Jamming and overpacking fuzzy microgels: deformation, interpenetration, and compression. *Sci. Adv.* **3**, e1700969 (2017).
29. Bachman, H. et al. Ultrasoft, highly deformable microgels. *Soft Matter* **11**, 2018–2028 (2015).
30. Virtanen, O. L. J., Mourran, A., Pinard, P. T. & Richtering, W. Persulfate initiated ultra-low cross-linked poly(*n*-isopropylacrylamide) microgels possess an unusual inverted cross-linking structure. *Soft Matter* **12**, 3919–3928 (2016).
31. Berthier, L., Moreno, A. J. & Szamel, G. Increasing the density melts ultrasoft colloidal glasses. *Phys. Rev. E* **82**, 060501 (2010).
32. Verso, F. L., Pomposo, J. A., Colmenero, J. & Moreno, A. J. Tunable slow dynamics in a new class of soft colloids. *Soft Matter* **12**, 9039–9046 (2016).
33. Kurzthaler, C., Leitmann, S. & Franosch, T. Intermediate scattering function of an anisotropic active Brownian particle. *Sci. Rep.* **6**, 36702 (2016).
34. Schwarz-Linek, J. et al. *Escherichia coli* as a model active colloid: a practical introduction. *Colloids Surf. B* **137**, 2–16 (2016).
35. Berne, B. J. & Pecora, R. *Dynamic Light Scattering: With Applications to Chemistry, Biology, and Physics* (Courier Corporation, 2000).
36. Cipelletti, L., Manley, S., Ball, R. & Weitz, D. Universal aging features in the restructuring of fractal colloidal gels. *Phys. Rev. Lett.* **84**, 2275 (2000).
37. Angelini, R. et al. Dichotomic aging behaviour in a colloidal glass. *Soft Matter* **9**, 10955–10959 (2013).
38. Ruta, B., Baldi, G., Monaco, G. & Chushkin, Y. Compressed correlation functions and fast aging dynamics in metallic glasses. *J. Chem. Phys.* **138**, 054508 (2013).

39. Angelini, R. et al. Glass–glass transition during aging of a colloidal clay. *Nat. Commun.* **5**, 4049 (2014).
40. Bouchaud, J.-P. & Pitard, E. Anomalous dynamical light scattering in soft glassy gels. *Eur. Phys. J. E* **9**, 287–291 (2002).
41. Cipelletti, L. et al. Universal non-diffusive slow dynamics in aging soft matter. *Faraday Discuss.* **123**, 237–251 (2003).
42. Duri, A. & Cipelletti, L. Length scale dependence of dynamical heterogeneity in a colloidal fractal gel. *Europhys. Lett.* **76**, 972–978 (2006).
43. Bouzid, M., Colombo, J., Barbosa, L. V. & Del Gado, E. Elastically driven intermittent microscopic dynamics in soft solids. *Nat. Commun.* **8**, 15846 (2017).
44. Pelaez-Fernandez, M., Souslov, A., Lyon, L., Goldbart, P. M. & Fernandez-Nieves, A. Impact of single-particle compressibility on the fluid-solid phase transition for ionic microgel suspensions. *Phys. Rev. Lett.* **114**, 098303 (2015).
45. Gao, J. & Frisken, B. Cross-linker-free *n*-isopropylacrylamide gel nanospheres. *Langmuir* **19**, 5212–5216 (2003).
46. Scotti, A. et al. Hollow microgels squeezed in overcrowded environments. *J. Chem. Phys.* **148**, 174903 (2018).

Acknowledgements

We thank F. Camerin, L. Cipelletti, C. Maggi, A. Ninarello and D. Truzzolillo for useful discussions and comments. We acknowledge support from the European Research Council (ERC Consolidator Grant 681597, MIMIC) and from ETN-COLLDENSE (H2020-MCSA-ITN-2014, grant 642774).

Author contributions

N.G. and E.Z. designed and performed the research, and wrote the paper.

Competing interests

The authors declare no competing interests.

Additional information

Supplementary information is available for this paper at https://doi.org/10.1038/s41567-019-0480-1.

Reprints and permissions information is available at www.nature.com/reprints.

Correspondence and requests for materials should be addressed to N.G. or E.Z.

Journal peer review information: *Nature Physics* thanks Grzegorz Szamel and the other anonymous reviewer(s) for their contribution to the peer review of this work.

Publisher's note: Springer Nature remains neutral with regard to jurisdictional claims in published maps and institutional affiliations.

Methods

Model and simulations. We model 2D soft particles as polymer rings interacting with the classical bead-spring model[47] with an additional internal elasticity. Each ring is composed of N_m monomers of diameter σ_m. Two bonded monomers at distance r interact through the sum of a Weeks–Chandler–Andersen (WCA) potential

$$V_{WCA}(r)=\begin{cases}4\varepsilon\left[\left(\frac{\sigma_m}{r}\right)^{12}-\left(\frac{\sigma_m}{r}\right)^{6}\right]+\varepsilon & \text{if} \quad r\le 2^{\frac{1}{6}}\sigma_m\\ 0 & \text{if} \quad r>2^{\frac{1}{6}}\sigma_m\end{cases} \tag{1}$$

and a finite extensible nonlinear elastic (FENE) potential

$$V_{FENE}(r)=-\varepsilon\ k_F R_F^2 \ln\left[1-\left(\frac{r}{R_F\sigma_m}\right)^2\right] \quad \text{if} \quad r<R_F\sigma_m \tag{2}$$

where $k_F=15$ is the spring constant, $R_F=1.5$ is the maximum extension of the bond and ε is the unit of energy. Non-bonded monomers interact with $V_{WCA}(r)$ only. To modulate the internal elasticity of the ring we add a Hertzian potential acting between each monomer and the centre of mass of the ring, as

$$V_H(r)=U(1-r/\sigma_H)^{5/2}\Theta(1-r/\sigma_H) \tag{3}$$

where U is the Hertzian strength in units of energy ε and σ_H is the distance at rest of each monomer from the centre of mass of the ring when the polymer ring is perfectly circular. We also define the diameter of the circle inscribing the polymer ring as $\sigma_{ring}=\sigma_H+\sigma_m$. Addition of the internal elasticity on the one hand avoids flattening of the rings on increasing the packing fraction and on the other hand provides a tunable softness to the ring. The smaller the Hertzian strength, the larger is the ability of the ring to deform (that is, higher softness), while with increasing U the ring behaviour will tend to that of a hard disk. Thus, crucially, the model takes into account particle deformation, which becomes more and more relevant at high densities (see Supplementary Information), with the inner Hertzian field playing the role of an effective many-body term.

In our study we investigate the static and dynamic properties of elastic rings for several values of U (100, 500, 1,000 and 3,000). We mainly show the results for $N=1{,}000$ elastic rings with $N_m=10$ monomers for which $\sigma_H=3.107\sigma_m$. However, we note that we also tested the cases of $N_m=5$ and $N_m=20$, for which we found similar results. In addition we also examined a larger system composed of $N=10{,}000$ rings and $N_m=10$ for selected high packing fractions (Supplementary Fig. 11). Due to the high propensity of the system to crystallize we use a size polydispersity of 12% both for σ_m and for σ_H according to a log-normal distribution.

We perform Langevin dynamics simulations at constant temperature with $k_BT=1$. As the unit of length we use the average ring diameter $\langle\sigma_{ring}\rangle$ at low dilution and as the unit of time $t_0=\langle\sigma_{ring}\rangle\sqrt{m_{ring}/\varepsilon}$, where $m_{ring}=m\times N_m$ (m is the monomer unit mass). A velocity Verlet integrator is used to integrate the equations of motion with a time step of $dt=10^{-3}$. We follow ref. [48] to model Brownian diffusion by defining the probability p that a particle undergoes a random collision every Y time steps for each particle. By tuning p it is possible to obtain the desired free particle diffusion coefficient $D_0=(k_BTYdt/m)(1/p-1/2)$. We fix $D_0=0.008$ but we also checked other values ranging from $D_0=0.0015$ to $D_0=0.08$, finding that there is no influence of the microscopic dynamics on the long-time behaviour (Supplementary Fig. 12). The packing fraction of the rings is defined as $\zeta=\sum_{i=1}^{N}\pi\sigma_{i,ring}^2/4L^2$, where $\pi\sigma_{i,ring}^2/4$ is the area of the ith ring at low dilution and L is the edge of the squared simulation box.

Ring deformation. To evaluate how polymer rings deform, we calculate the gyration tensor, from which we extract the radius of gyration $R_g=\left[\frac{1}{N_m}\sum_{i=1}^{N_m}(\mathbf{r}_i-\mathbf{r}_{CM})^2\right]^{1/2}$, where $\mathbf{r}_{CM}$ is the centre of mass of the ring. We also calculate the asphericity parameter as $a=(\lambda_2-\lambda_1)^2/(\lambda_1+\lambda_2)^2$ where λ_1 and λ_2 are the eigenvalues of the gyration tensor[49]. In addition, we estimate the effective packing fraction ϕ occupied by the rings by calculating the average area (A_R) of rings from the gyration radius of each ring or from the area of the ellipse having as semi-axis the eigenvectors extracted from the gyration tensor. As both approaches yield similar results, we use the average of the two. Once the area is calculated, we define the effective packing fraction as $\phi=\zeta A_R/A_{R_0}$, where A_{R_0} is the average value of the area of a ring at low dilution.

Ring dynamics. We quantify the dynamics of the rings by evaluating the MSD $\left\langle r^2(t)\right\rangle=\left\langle\frac{1}{N}\sum_{i=1}^{N}(\mathbf{r}_{CM}^i(t)-\mathbf{r}_{CM}^i(t=0))^2\right\rangle$ (where $\langle\ldots\rangle$ denotes an ensemble average) and the self-intermediate scattering function $F_s(q^*,\ t)=\left\langle\frac{1}{N}\sum_{i=1}^{N}e^{i\mathbf{q}^*\cdot(\mathbf{r}_{CM}^i(t)-\mathbf{r}_{CM}^i(t=0))}\right\rangle$. Both observables are calculated using the positions of the centres of mass of the rings. It is well established that the long-time decay of $F_s(q^*,t)$ can be described by a generalized exponential decay $F_s(q^*,t)\sim\exp(-(t/\tau_\alpha)^\beta)$ modulated by a shape parameter β. To extract the value of β and τ_α, we approximate the whole $F_s(q^*,t)$ as the sum of two exponentials:

$$F_s(q^*,\ t)=C\ \exp(-t/\tau_0)+(1-C)\exp(-(t/\tau_\alpha)^\beta) \tag{4}$$

where the first one is a simple exponential that accounts for the short-time decay controlled by τ_0 and the second provides a description of the long-time decay, with C a constant varying between 0 and 1. When the dynamics becomes very fast at high ζ, only the second exponential is retained in equation (4), being a single compressed exponential able to interpolate the whole curve.

Analysis of fast rings. At high ζ we divide the total simulation time into windows of duration Δt of the order of τ_α. In particular we fix $\Delta t=7.88$ in reduced units and we select the 10% fastest particles in each window. We then calculate the MSD only for these particles, starting from the interval where they were selected. The dynamics of the fastest rings, quantified by their MSD averaged over all considered windows, is faster than that of all rings; that is, it can be described by a larger γ exponent of the superdiffusive behaviour in the MSD that is found to be close to 1.9. However, at larger times, they always retain diffusive behaviour. It is important to note that, despite the large polydispersity of the system, the fastest particles are evenly distributed among all particle sizes. Analysing different time windows, we find that for the considered state point ($U=1{,}000$ and $\zeta=1.264$) the super-diffusive exponent is exactly equal to 2, signalling purely ballistic dynamics, for about 25% of the considered time intervals. This ratio strongly depends on the chosen state point and on the number of considered fastest rings. Indeed, for each interval, we can always define a subset of fastest rings undergoing purely ballistic dynamics; their number increases with increasing ζ and increasing U, thus explaining the behaviour of the average value of γ, reported in Supplementary Fig. 4, and also of the shape parameter β, shown in Fig. 1d.

Modified Angell's plot. In standard glass-formers an Angell's plot reports the variation of the viscosity or relaxation time of the system in a logarithmic scale versus the control parameter driving the glass transition, for example the packing fraction in the case of colloidal suspensions, appropriately rescaled by its glass transition value[14–16]. In our system, we do not find a glass transition, but the system undergoes a reentrant melting. We thus use the value of ζ_R as the rescaling packing fraction and visualize the dependence on the relaxation time on ζ, approaching this value both from above and from below. However, rings with different softness U have different relaxation times at ζ_R, so it is more convenient to use a packing fraction ζ^* that is slightly different but close to ζ_R and dependent on U, for which a common value of τ_α is found. This allows us to scale, altogether, the data for different values of U. In the main text we report results where we have chosen the common value $\tau_\alpha\simeq 650$ in reduced units, but we have verified that different choices provide qualitatively similar results.

Data availability

The data sets generated and/or analysed during the current study are available from the authors upon reasonable request.

Code availability

The computer code is available from the authors upon reasonable request.

References

47. Grest, G. S. & Kremer, K. Molecular dynamics simulation for polymers in the presence of a heat bath. *Phys. Rev. A* **33**, 3628 (1986).
48. Russo, J., Tartaglia, P. & Sciortino, F. Reversible gels of patchy particles: role of the valence. *J. Chem. Phys.* **131**, 014504 (2009).
49. Rudnick, J. & Gaspari, G. The asphericity of random walks. *J. Phys. A* **19**, L191–L193 (1986).